Laser and Particle Beams (2017), *35*, 1–9.

doi:10.1017/S0263034616000732

A comparative study of Cu–Ni Alloy using LIBS, LA-TOF, EDX, and XRF

N. AHMED,[1,2] R. AHMED,[1] M. RAFIQE,[2] AND M.A. BAIG[1]

[1]National Centre for Physics, Quaid-i-Azam University Campus, 45320 Islamabad, Pakistan
[2]Department of Physics, University of Azad Jammu and Kashmir, Muzaffarabad, Azad Kashmir, Pakistan

(Received 1 July 2016; Accepted 25 October 2016)

Abstract

LASER induced breakdown spectroscopy (LIBS) has been used for the quantitative analysis of Cu–Ni alloy of known composition (75% Cu, 25% Ni) using the one line calibration free-LIBS (OLCF-LIBS), self-calibration-LIBS (SC-LIBS), calibration free LIBS (CF-LIBS), time of flight-mass spectroscopy (TOF-MS), energy dispersive X-ray spectroscopy (EDX) and X-ray fluorescence spectroscopy (XRF). For the LIBS-based studies, the plasma was generated by focusing the beam of a Q-switched Nd:YAG laser (532 nm, pulse energy about 200 mJ, 5 ns pulse duration) while the sample was placed in air at an atmospheric pressure. Plasma temperature about (9500 ± 300) K was calculated by the Boltzmann plot method using the neutral lines of Cu and Ni whereas the electron number density was calculated $(2.0 \pm 0.5) \times 10^{16}$ cm^{-3} from the Stark broadening of an isolated Cu line as well as using the relative intensities of the neutral and singly ionized optically thin lines in the Saha–Boltzmann equation. The elemental compositions determined by different LIBS methods and standard techniques are; OLCF-LIBS (69% Cu and 31% Ni), SC-LIBS (72% Cu and 28% Ni), CF-LIBS (74% Cu and 26% Ni), TOF (74% Cu and 26% Ni), EDX (75% Cu and 24.5% Ni), XRF (73% Cu and 24.7% Ni), and LA-TOF (74% Cu and 26% Ni). It is demonstrated that the CF-LIBS method gives compositions comparable with that determined by LA-TOF, EDX, or XRF, which is also in agreement with the certified reported composition.

Keywords: CF-LIBS; CuNi alloy; Electron density; LA-TOFMS; LIBS; Plasma temperature; Quantitative analysis

1. INTRODUCTION

Laser induced breakdown spectroscopy (LIBS) is an analytical technique that is being applied in industry (Noll *et al.,* 2001; Noll *et al.,* 2014), environmental diagnostics (Bassiotis *et al.,* 2001; Bulajic *et al.,* 2001), and biomedical research (Bassiotis *et al.,* 2001; Singh & Rai, 2001). In this technique a high-power pulsed laser is focused on the surface of a solid (Gomba *et al.,* 2001; Fichet *et al.,* 2003; Hafeez *et al.,* 2008; Baig *et al.,* 2012), liquid (Charfi & Harith, 2002; Fichet *et al.,* 2003; Mohamed, 2007) or in the gaseous target (Hohreiter & Hahn, 2005) to generate plasma. Elemental composition of any material can be obtained from the emission spectrum of the laser produced plasma (Cremers & Radziemski, 2006; Hahn & Omenetto, 2012). For the last couple of decades, LIBS technique has been used for the qualitative and quantitative analysis (Ciucci *et al.,* 1999; Bassiotis *et al.,* 2001; Fichet *et al.,* 2003; Winefordner *et al.*, 2004; Ahmed *et al.,* 2015; Ahmed & Baig 2015) by the calibration curves method (Galbacs *et al.*, 2001) and by the calibration free (CF) methods (Galbacs *et al.*, 2001; Hohreiter & Hahn 2005; De Giacomo *et al.,* 2007*a*, *b*; Tognoni *et al.*, 2010; Unnikrishnan *et al.,* 2012). In the calibration curve method, reference samples are needed for drawing the calibration curves between the emission lines intensities versus the known compositions. The composition of the unknown samples is then estimated by comparing the emission line intensity from the calibration curves (Bassiotis *et al.,* 2001; Fichet *et al.,* 2003; Gupta *et al.*, 2011; Unnikrishnan *et al.,* 2012; Ahmed *et al.,* 2015). Limitation of this method is that, only samples with similar compositions can be analyzed quantitatively. However, in the CF-IBS method, no reference samples are needed (Gomba *et al.,* 2001; Burakov & Raikov, 2007; Aguilera *et al.,* 2009; Tognoni *et al.*, 2010; Unnikrishnan *et al.,* 2012). For the quantitative analysis of a sample, the plasma needs to be optically thin (Unnikrishnan *et al.*, 2010), and fulfills the local thermodynamic equilibrium (LTE) condition (Cristoforetti *et al.*, 2010). In the one-line calibration free LIBS (OLCF-LIBS) method, only a single

Address correspondence and reprint requests to: M.A. Baig, National Centre for Physics, Quaid-i-Azam University Campus, 45320 Islamabad, Pakistan. E-mail: baig@qau.edu.pk; baig77@gmail.com

spectral line is used to measure the elemental composition. Whereas, to draw a Boltzmann plot for the determination of plasma temperature and composition, at least four to five optically thin spectral lines are required. However, in the case of trace elements, it is always difficult to find sufficient number of optically thin lines, which limits the use of the Boltzmann plot method for the quantitative analysis of the trace elements in the target material. To overcome this difficulty Gomba *et al.* (2001) developed a new CF-LIBS technique in which concentration of the elements can be estimated by comparing the theoretically obtained electron density and the ratio of the number densities of neutral and the singly ionized species of the same elements as well as of the different elements with the experimentally measured electron densities. However, accurate values of the electron density n_e and temperature T_e are important in CF-LIBS. The electron temperature T_e can be deduced from the Boltzmann plot method (Joseph *et al.*, 1994; Gomba *et al.,* 2001; El Sherbini & Saad Al Aamer, 2012) and electron number density n_e can be calculated from the Stark broadening of the spectral lines (Borgia *et al.*, 2000; Cremers & Radziemski, 2006) or by the Saha–Boltzmann equation (Borgia *et al.*, 2000; Andrzej *et al.*, 2006; Unnikrishnan *et al.,* 2012).

Copper (Cu) and nickel (Ni) are adjacent elements in the Period Table. The Cu–Ni alloy is highly resistant to corrosion therefore it is used in marine applications. A typical Cu–Ni alloy with 75% copper and 25% nickel is used in new strewn coins. The main objectives of the present work were to exploit the LIBS as well as other techniques for the quantitative analysis of the Cu–Ni alloy, which is used to make the Pakistani five rupee coin of year 2004 and to compare it with its certified composition. Quantitative results obtained using three LIBS-based techniques; OLCF-LIBS (Andrea *et al.*, 2015), SC-LIBS (Ciucci *et al.*, 1999), CF-LIBS (Unnikrishnan *et al.*, 2012) are compared with that obtained by the XRF, EDX, and LA-TOF techniques showing good agreement.

2. EXPERIMENTAL SETUP

The experimental details for recording the optical emission spectrum of the laser produced plasma are the same as described in our earlier papers (Hafeez *et al.,* 2008; Ahmed & Baig, 2009; Baig *et al.,* 2012; Shaikh *et al.*, 2013; Ahmed *et al.*, 2015). In brief, for the ablation of the target sample we have used a high-power Q-switched Nd:YAG laser (Brilliant-B-Quantal, France) having 5 ns pulse duration and 10 Hz repetition rate. The laser pulse energy is about 850 mJ at 1064 nm and about 500 mJ at 532 nm. Using the LIBS software, the laser pulse energy can be changed by varying the Q-switch delay whereas the laser energy has been measured by an energy meter (Nova-Quantal, France). A quartz lens (convex) of 20 cm focal length was used to focus the laser beam on the target sample placed in air at an atmospheric pressure. The sample was placed on a rotating stage that was kept rotating around an axis; to prevent the formation of deep craters, to provide a fresh location of target sample for the energy single shot, for the improvement of reproducibility of mass ablation and to avoid the non-uniformly of the target. In order to prevent the air breakdown in front of the sample, it was necessary to keep the distance between the lens and the sample less than the focal length (<20 cm). The optical fiber (high – OH, core diameter about 600 μm) was used to collect the plasma radiation with a collimating lens (0°–45° field of view), which was placed normal to the laser beam. The emitted radiation was guided to the spectrometer through the fiber optics and then detected by the system software. There are four spectrometers each having width of 10 μm in the detection system (Avantes, Holand), which covers the wavelength range of 250–870 nm. To correct the emission signal, we subtracted the dark signal of the detector using the LIBS software. Three LIBS-based methods are employed for quantitatively analyzing the LIBS spectra, One line calibration LIBS (OLC-LIBS), self-calibration LIBS (SC-LIBS), and CF-LIBS. The same Pakistani five rupee coin of year 2004 was quantitatively analyzed by using the Bruker S8 Tiger X-ray fluorescence (XRF) spectrometer, by the EDX spectrometer attached with Quanta 450 FEG scanning electron microscope, and by a locally fabricated laser ablation/ionization time-of-flight mass spectrometer (TOF-MS).

3. RESULTS AND DISCUSSIONS

3.1. Emission Studies

The plasma on the surface of the sample was generated by focusing the beam of a Nd:YAG laser at 532 nm, pulse energy 130 mJ. As soon as the plasma is generated, the plasma plume expands perpendicular to the target surface and after a few micro seconds, it cools down. The emission from the plasma plume contains characteristics spectral lines of the constituent elements. The time delay of 2 μs between the laser pulse and the detection system was opted to reduce the continuum contribution. In Figures 1–3, the emission spectra of the laser produced Cu–Ni alloy plasma are presented covering the wavelength region from 200 to 700 nm. The major part of Figures 1–3 consists of spectral lines of copper and nickel as the alloy mainly contains these elements. The dominating lines belong to neutral copper and nickel. Besides, a couple of lines attached to the singly ionize copper and nickel are observed.

3.2. Determination of Plasma Temperature

We have determined the plasma temperature from the relative intensities of the emission lines of copper and nickel using the Boltzmann plot method (Borgia *et al.*, 2000). The observed emission spectra contain spectral lines of CuI at 296.11, 450.93, 453.96, 458.69, 510.55, 515.32, 570.02, 578.21 and 521.82 nm; and that of NiI at 490.44, 300.25,

https://doi.org/10.1017/S0263034616000732 Published online by Cambridge University Press

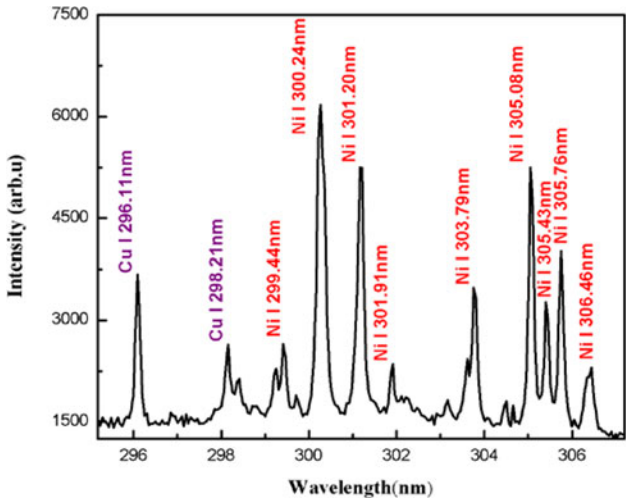

Fig. 1. Optical emission spectrum of the laser produced Cu–Ni alloy plasma covering the spectral region 295–307 nm. The spectral lines of Cu I and Ni I are assigned in the blue and red color, respectively.

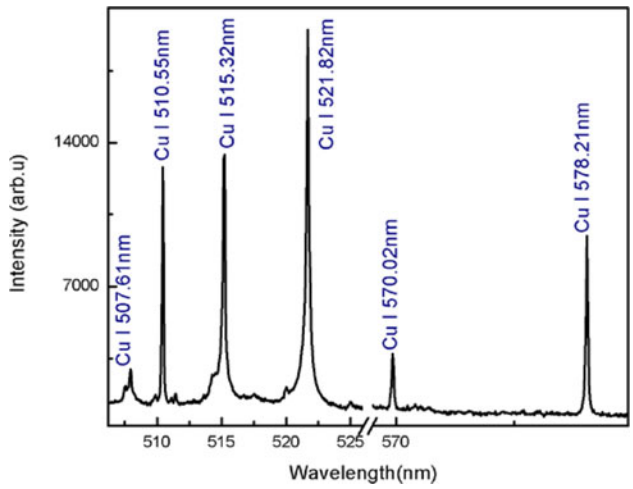

Fig. 3. Optical emission spectrum of the laser produced Cu–Ni alloy plasma covering the spectral region 506–579 nm. All the lines belong to neutral copper.

301.20, 305.08, 339.30, 344.62, 345.85, 346.16, and 356.64 nm, which have been used to construct the Boltzmann plot to extract the plasma temperature. We have selected the optically thin lines in the Boltzmann plot that are free from self-absorption (Harilal *et al.*, 2005; De Giacomo *et al.*, 2007*a*, *b*; Cristoforetti *et al.,* 2010). To validate the condition for the optically thin plasma from the observed emission spectrum, we have used the experimentally observed intensity ratio of various spectral lines of CuI and NiI and compared it with the ratio of their transition probabilities (Unnikrishnan *et al.*, 2012). We used three pairs of lines in CuI at 515.32 and 521.82 nm, 470.45 and 529.25 nm, 510.55 and 515.32 nm; and one pair of lines of NiII at 254.66 and 251.163 nm. The experimentally observed and the theoretically calculated values agree with in 10% uncertainty, which supports the optically thin plasma assertion.

The atomic parameters of the selected lines were taken from NIST database that are listed in Table 1. The Boltzmann plots for copper and nickel are presented in Figure 4. The plasma temperatures have been extracted from the slopes of the straight lines, which yields the value for copper as 9535 ± 300 K and for nickel 9455 ± 300 K. The errors in the deduced plasma temperatures mainly come from the uncertainties in the transition probabilities and in the measurement of the line intensities. For the quantitative analysis, we have used an average value of the plasma temperature 9500 ± 300 K.

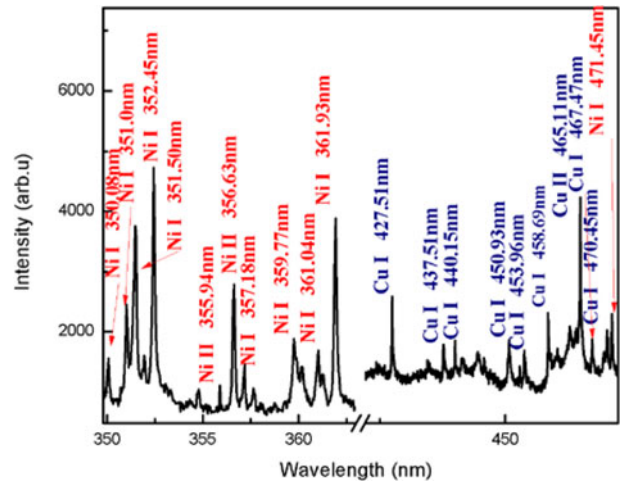

Fig. 2. Optical emission spectrum of the laser produced Cu–Ni alloy plasma covering the spectral region 350–475 nm. The spectral lines of CuI, II and NiI, Ni II are assigned in blue and red color, respectively.

3.3. Determination of Electron Number Density

One of the commonly used methods to calculate the electron number density is from the measured Stark broadening of neutral or singly ionized spectral lines. The electron number density (N_e) is related to the full-width at half-maximum (FWHM) of a Stark broadened line as (Borgia *et al.*, 2000; Cremers & Radziemski, 2006):

$$n_e(\mathrm{cm}^{-3}) = \left(\frac{\Delta\lambda^{S}_{FWHM}}{2\omega_s(\lambda, T_e)}\right) \times N_r, \quad (1)$$

where $\Delta\lambda^{S}_{FWHM}$ is the Stark contribution to the total line profile, ω_s is the Stark broadening parameter, which is slightly wavelength and temperature dependent and its values are available in the literature, and N_r is the reference electron density, which is equal to 10^{16} (cm^{-3}). The Stark line widths $\Delta\lambda^{S}_{FWHM}$ of the spectral lines have been determined by deconvoluting the observed line profiles as a Voigt profile, which takes into account the instrumental width and the Doppler broadening. The line profile of the optically thin line of CuI at 510.55 nm was selected to calculate the electron

https://doi.org/10.1017/S0263034616000732 Published online by Cambridge University Press

Table 1. *Spectroscopic parameters of the emission lines of copper and nickel (NIST data base) to construct the Boltzmann plot.*

Wavelength λ (nm)	Transition		Transition probability (10^{7s-1})	E_k (eV)	g_k	G_i
	Upper level	Lower level				
Cu						
296.11	$3d^9 4s4p\ ^2F_{7/2}$	$3d^9 4s^2\ ^2D_{5/2}$	0.376	5.57	8	6
450.93	$3d^9 4s5s\ ^4D_{1/2}$	$3d^9 4s4p\ ^4F_{3/2}$	2.75	7.99	2	4
453.97	$3d^9 4s)5s\ ^4D_{3/2}$	$3d^9 4s4p\ ^4F_{5/2}$	2.12	7.88	4	6
458.69	$3d^9 4s5s\ ^4D_{5/2}$	$3d^9 4s4p\ ^4F_{7/2}$	3.20	7.80	6	8
510.55	$3d^{10} 4p\ ^2P_{3/2}$	$3d^9 4s^2\ ^2D_{5/2}$	2.0	3.82	4	6
515.32	$3d^{10} 4d\ ^2D_{3/2}$	$3d^{10} 4p\ ^2P_{1/2}$	6.0	6.19	4	2
521.82	$3d^{10} 4d\ ^2D_{5/2}$	$3d^{10} 4p\ ^2P_{3/2}$	7.5	6.19	6	4
570.02	$3d^{10} 4p\ ^2P_{3/2}$	$3d^9 4s^2\ ^2D_{3/2}$	0.024	3.82	4	4
578.21	$3d^{10} 4p\ ^2P_{1/2}$	$3d^9 4s^2\ ^2D_{3/2}$	0.165	3.79	2	4
Ni						
300.24	$3d94s\ ^3D_3$	$3d^8 4s4p\ ^3D_3$	8.0	4.15	7	7
301.20	$3d^9 4s\ ^1D_2$	$3d^8 4s4p\ ^1D_2$	13.0	4.54	5	5
305.08	$3d^9 4s\ ^3F_4$	$3d^8 4s4p\ ^3D_3$	6.0	4.09	9	7
339.30	$3d^9 4s\ ^3D_3$	$3d^9 4p\ ^3F_3$	2.4	3.68	7	7
344.63	$3d^9 4s\ ^3D_2$	$3d^9 4p\ ^3D_2$	4.4	3.71	5	5
345.85	$3d^9 4s\ ^3F_2$	$3d^9 4p\ ^3D_1$	6.1	3.80	5	3
346.16	$3d^9 4s\ ^5F_4$	$3d^8 4s4p\ ^3D_3$	2.7	3.61	9	7
356.64	$3d^9 4s\ ^1D_2$	$3d^9 4p\ ^1D_2$	5.6	3.90	5	5
490.44	$3d^9 4p\ ^2[1/2]_1$	$3d^9 4d\ ^3P_2$	6.2	6.07	3	5

number density using the impact broadening parameter ω = 0.0139 nm listed in (Konjevic & Knjević, 1986; Babina *et al.*, 2003). In Figure 5, we show the experimental observed data points as dots and the full line, which passes through all the experimental points is the Voigt function fit. The instrumental width of our spectrometer is 0.06 ± 0.02 nm and the Doppler width is estimated at an elevated temperature 9500 K as 0.004 nm, which is very small and can be neglected. The electron number density is calculated as (2.2 ± 0.5) × 10^{16} cm^{-3}.

3.4. Number Density Measurement using the Saha–Boltzmann Relation

The Saha–Boltzmann equation relates the number density of a particular element in the two consecutive charged states Z and $Z + 1$ (Tognoni *et al.*, 2007; Unnikrishnan *et al.*, 2012):

$$n_e \frac{n^{\alpha,z+1}}{n^{\alpha,z}} = 6.04 \times 10^{21} (T_{eV})^{3/2} \frac{P_{\alpha,z+1}}{P_{\alpha,z}} \exp\left[-\frac{\chi_{\alpha,z}}{k_B T}\right], \quad (2)$$

where n_e (cm^{-3}) is the electron density, $n^{\alpha,z+1}$ is the density of atoms in the upper charged state $z + 1$ of the element α,

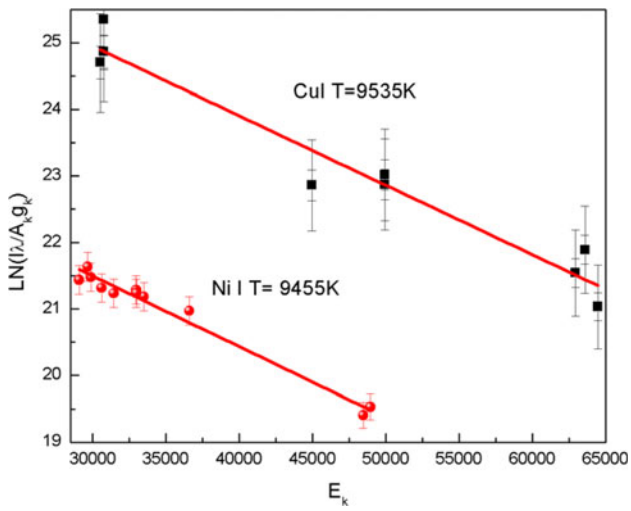

Fig. 4. Typical Boltzmann plots for estimating the plasma temperature. Emission lines from singly ionized Cu and Ni are used for obtaining temperature.

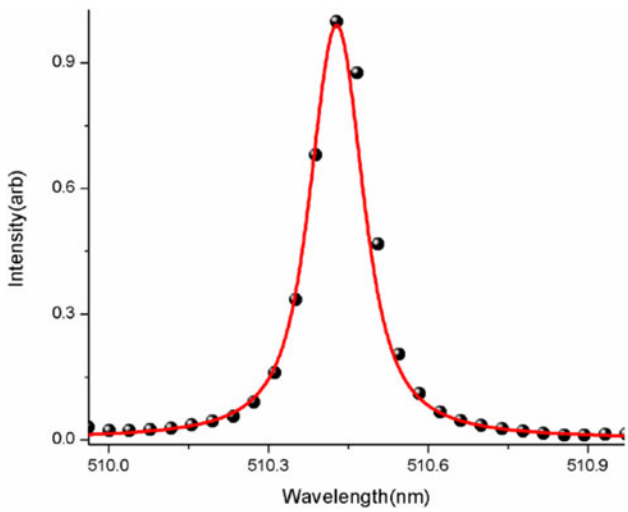

Fig. 5. Stark broadened line profile of copper line at 510.55 nm along with the Voigt fit.

https://doi.org/10.1017/S0263034616000732 Published online by Cambridge University Press

$n^{\alpha,z}$ is the density of atoms in the lower charged state z of the same element α, $\chi_{\alpha,z}$ (eV) is the ionization energy of the element α in the charged state z, $P_{\alpha,z+1}$ and $P_{\alpha,z}$ are the partition functions of the upper charged state $z+1$ and of the lower charged state z respectively, whereas $T_{(eV)}$ is the plasma temperature in electron volt. This equation can also be written in terms of intensities of the atomic and the ionic lines as (Tognoni *et al.*, 2007; Unnikrishnan *et al.*, 2012)

$$n_e = 6.04 \times 10^{21} \times \frac{I_z}{I_{z+1}} (T_{eV})^{3/2} \exp\left[\frac{-E_{k,\alpha,z+1} + E_{k,\alpha,z} - \chi_{\alpha,z}}{k_B\, T}\right], \tag{3}$$

where $E_{k,\alpha,z}$ is the upper level energy of the element α in the charged state z, $E_{k,\alpha,z+1}$ is the upper level energy of the element α in the charged state $z+1$ and $I_z = \lambda_{ki}\ I_{ki}/A_{ki}\ g_k$. The electron density was obtained using the intensity ratio of the neutral and singly ionized spectral lines of Ni. The plasma temperature is taken as 0.82 eV and the ionization energy is 7.64 eV (De Giacomo *et al.*, 2007*a*, *b*; Gomba *et al.*, 2001). Substituting the numerical values in Eq. (3), we have determined the value of n_e from the two NiII lines at 251.09 and 254.66 nm, whereas a number of neutral nickel lines were used. The estimated electron densities were determined in the range from 1.4 to 2.8×10^{16} cm^{-3}. However, an average value $n_e = (2.0 \pm 0.3) \times 10^{16}$ has been used in the subsequent calculations.

The McWhirter criterion has also been validated for the CuI line at 450.93 nm and NiI line at 493.73 nm to check how close the plasma is to the LTE. For a stationary and homogeneous plasma, the collisional mechanism dominates over the radiative process, therefore, a lower limit for the electron density, which satisfy the LTE condition is (Cristoforetti *et al.*, 2010):

$$N_e \geq 1.6 \times 10^{12} \times \Delta E^3 \times T^{1/2}. \tag{4}$$

Here ΔE is the energy difference between the upper and lower energy level and T is the plasma temperature. The electron density is calculated as 1.1×10^{14} cm^{-3}, which is much lower than that determined from the Stark broadened spectral lines of copper. Thus our plasma is not far from LTE.

3.5. One Line CF Method for Quantitative Analysis (OLCF-LIBS)

The Boltzmann equation, which links the intensities of emission lines emitted by the same species can be written as (Andrea *et al.*, 2015; Andrzej *et al.*, 2006):

$$FC^z = I_k \frac{U^z(T)}{A_k g_k} e^{(E_k/k_B T)}, \tag{5}$$

where the F factor is related to the ablated mass (constant for constant efficiency of the spectral system), I_k is the line intensity, C^z is the concentration of neutral atom, A_k is the transition probability, g_k is the statistical weight of the upper level, $U(T)$ is the partition function, E_k is the energy of the upper level, k is the Boltzmann constant, and T is the electron temperature in eV. The factor F can be determined by normalizing the species concentration. At an average plasma temperature 0.82 eV, the partition functions of Cu and Ni are $U(I)_{Cu} = 3.93$, $U(II)_{Cu} = 1.58$, and $U(I)_{Ni} = 40.08$, $U(II)_{Ni} = 18.48$ (NIST database). An average value of electron density is deduced as: $n_e = 2.0 \times 10^{16}$ cm^{-3}. The value of concentration of neutral atoms C_z is calculated from the above Eq. (5) and the concentration of the ionized atoms C_{z+1} is calculated using the Saha–Boltzmann equation, relating the concentrations in the two consecutive charge states Z and $Z+1$ of a particular element

$$n_e \frac{C^{z+1}}{C^z} = \frac{(2m_e kT)^{3/2}}{h^3} \frac{2U_{z+1}}{U_z} \exp\left[-\frac{E_{ion}}{kT}\right] \text{cm}^{-3}. \tag{6}$$

Equation 6 gives the ratio the concentration of two charge states Z and $Z+1$ of the same element (C^{z+1}/C^z) (Unnikrishnan *et al.*, 2012; Andrea *et al.*, 2015), from here we can easily calculate the value of C^{z+1} by substituting the value of C^z obtained from Eq. (5).

Total concentration of Cu and Ni is presented as: $C_t^{Cu} = C_z^{Cu} + C_{z+1}^{Cu}$, $C_t^{Ni} = C_z^{Ni} + C_{z+1}^{Ni}$.

To calculate the percentage compositions, we used the following relations:

$$C^{Ni}\% = \frac{n_{tot}^{Ni} \times 58.69}{n_{tot}^{Ni} \times 58.69 + n_{tot}^{Cu} \times 63.54} \times 100, \tag{7}$$

$$C^{Ni}\% = \frac{n_{tot}^{Cu} \times 63.54}{n_{tot}^{Ni} \times 58.69 + n_{tot}^{Cu} \times 63.54} \times 100. \tag{8}$$

This procedure yields the concentration of Cu as 69% and that of Ni as 31% with about 6% error.

3.6. Self-calibration Method for Quantitative Analysis (SC-LIBS)

For the quantitative analysis of the Cu–Ni alloy, the SC-LIBS method was also used (Borgia *et al.*, 2000). The Boltzmann plots were drawn for each element Cu and Ni separately. Initially the intercepts were determined from the Boltzmann plots of Ni and Cu and an average value of the electron temperature was deduced as 0.82 eV as shown in Figure 6.

The population of an excited level is related to the total density of neutral atoms or ions of an element by the Boltzmann equation as:

$$\ln\left[\frac{\lambda_{ki}\, I}{hc\, A_{ki} g_k}\right] = -\frac{E_k}{k_B\, T} + \ln\left[\frac{FC^s}{Z(T)}\right], \tag{9}$$

where I is the integrated line intensity, C^s is the concentration of the emitting atomic species and F is an experimental

https://doi.org/10.1017/S0263034616000732 Published online by Cambridge University Press

factor, which takes into account the efficiency of the collection system and volume of the plasma. This relation is a linear straight line equation of the form:

$$y = mx + q_s,$$

where

$$y = \ln\left[\frac{\lambda_{ki}\, I}{hc\, A_{ki} g_k}\right]; x = E_k \; ; m = -\frac{1}{k_B\, T}\; ; q_s = \ln\left[\frac{FC^s}{Z(T)}\right],$$

From the above expressions it can be written as

$$FC^s = U(T)e^{q_s}. \tag{10}$$

The Boltzmann plots were drawn for each element Cu and Ni separately. As the plasma fulfills the LTE condition, therefore all the Boltzmann plots possess nearly the same slope "*m*" but with different intercepts 'q_s'. The intercepts of the Boltzmann plot is related to the logarithm of the species concentration. The neutral lines of Ni and Cu were used to estimate the FC_I^s values for each species and the values of FC^{NiI} (or n^{NiI}) and FC^{CuI} (or n^{CuI}) were deduced.

Due to the insufficient number of observed lines of NiII and CuII, it was not possible to draw the Boltzmann plot for the singly ionized species, separately. Thus, the Saha–Boltzmann equation was used for estimating the values of $FC^{Ni\ I}$ (or n^{NiII}) and FC^{CuII} (or n^{CuII}) as below.

$$\frac{n^{\alpha,z+1}}{n^{\alpha,z}} = \frac{6.04\times10^{21}(T_{eV})^{3/2}(P_{\alpha,z+1}/P_{\alpha,z})\exp[-\chi_{\alpha,z}/k_BT]}{n_e}. \tag{11}$$

The total concentration of an element is the sum of the concentrations of the neutral and the ionize species. The concentration for each species is then determined from the relation (Borgia *et al.*, 2000; Ciucci *et al.*, 1999).

$$C^s_{total} = C^s_I + C^s_{II}. \tag{12}$$

The experimental factor F can be obtained by normalizing the sum of the concentration of all the species to unity as $\sum^{C}_{total} = 1$.

Finally, by adopting the above procedure the composition of the Cu–Ni alloy has been estimated; as Cu = 72% and Ni = 28% with about 3% error. The results are listed in Table 2. The agreement between the derived and the actual concentrations is good as compared with that derived in the previous LIBS-based method.

3.7. Quantitative Analysis by the CF Method (CF-LIBS)

After estimating the plasma temperature and the electron number density, the density ratios of the species of the same element were calculated using Eq. (2) and the value of n_e was obtained from the Saha–Boltzmann equation as presented in Eq. (13). For different elements α and β in different charge states Z and $Z+1$ respectively, the density ratios have been calculated as described by Gomba *et al.* (2001) and Unnikrishnan *et al.* (2012).

Table 2. *Quantitative calculation by self-calibration method.*

Parameters	Cu	Ni
q_s	28.23	24.80
U(I)	3.93	40.08
U(II)	1.58	18.48
χ	726	7.640
n^i	7.14×10^{12}	2.36×10^{12}
n^{ii}	5.40×10^{13}	2.28×10^{13}
n^t	6.12×10^{13}	2.52×10^{13}

$$\frac{n^{\alpha,z}}{n^{\beta,z+1}} = \frac{I_{z,\alpha}}{I_{z+1,\beta}}\times\frac{P_{\alpha,z}}{P_{\beta,z+1}}\exp\left[\frac{-E_{k,\beta,z+1}+E_{k,\alpha,z}}{k_BT}\right], \tag{13}$$

where $E_{k,\alpha,z}$ is the upper level energy of the element α in the charged state z, $E_{k,\beta,z+1}$ is the upper level energy of the element β in the charged state $z+1$and I_z is the measured intensity using $I_z = \frac{\lambda_{ki}\overline{I_{ki}}}{A_{ki}g_k}$. Four optically thin lines of CuI and NiII were used to calculate the n^{CuI}/n^{NiII} ratio and an average value is determined as 0.37. These results are tabulated in Table 3.

Substituting the average value of n_e into Eq. (2), we obtained the experimental values of n^{NiII}/n^{NiI} and n^{CuII}/n^{CuI} as 9.10 and 7.14, respectively.

To calculate the theoretical values of n_e and the ratio of number densities of the same elements n^{NiII}/n^{NiI} and n^{CuII}/n^{CuI} as well as the ratio of the number densities of different elements $n^{cuI}/n^{NiII,}$ we have used an algorithm (Unnikrishnan *et al.*, 2012) MATLAB program.

In brief, we used the estimated value of the plasma temperature T(eV), and the initially supposed values of $n_{t,Cu,}$ $n_{t,Ni}$, and n_e in this algorithm. The algorithm was stopped where the theoretical value of n_e converges. In the next step, we use the converged value of n_e, determined in the previous step as the starting value and the algorithm yields the converged values of $n_{t,Cu}$, $n_{t,Ni}$. In the next step, the converged values of n_e, $n_{t,Cu}$, and $n_{t,Ni}$ were used to calculate the density ratios of n^{NiII}/n^{NiI}, n^{CuII}/n^{CuI}, and n^{CuI}/n^{NiII}. The algorithm will stop where the theoretical ratios match with the experimentally found ratios n^{NiII}/n^{NiI}, n^{CuII}/n^{CuI}, and n^{CuI}/n^{NiII}.

In Table 4, we enlist the experimental as well as the theoretical values of these ratios showing a good agreement.

The optimized values of the total densities of nickel and copper are deduced as $n^{Ni}_{tot} = 1.0\times10^{16}$ and $n^{Cu}_{tot} = 2.6\times10^{16}$, respectively. Using these density values, the weighted concentrations were estimated as: $C^{Ni} = 26\%$ and $C^{Cu} = 74\%$ with 1% error.

https://doi.org/10.1017/S0263034616000732 Published online by Cambridge University Press

Table 3. *The density ratio (n^{cuI}/n^{NiII}) for the calibration free quantitative analysis.*

Cu I λ	I' (10^{-2}) *Cu*	P(I) *Cu*	E_k(eV) *Cu*	Ni II λ	I'(10^{-2}) *Ni II*	P(II) *Ni II*	E_k(eV) *Ni II*	$T_{(eV)}$	Average $n^{cu\ I}/n^{Ni\text{-}II}$
515.32	8.51	3.93	5.52	254.66	1.80	18.48	6.73	0.82	
521.82	0.32	3.93	6.87	254.66	1.80	18.48	6.73	0.82	0.37
515.32	8.51	3.93	5.52	251.16	4.74	18.48	6.62	0.82	
521.82	0.32	3.93	6.87	251.16	0.47	18.48	6.62	0.82	

Table 4. *Comparison of the experimentally and theoretically values derived at 0.82 eV plasma temperature.*

	Experimental values	Theoretical values
n_e (cm^{-3})	2.00×10^{16}	2.04×10^{16}
N^{NiII}/n^{NiI}	9.1	8.93
N^{CuI}/n^{NiII}	0.37	0.36
N^{CuII}/n^{CuI}	7.1	7.0

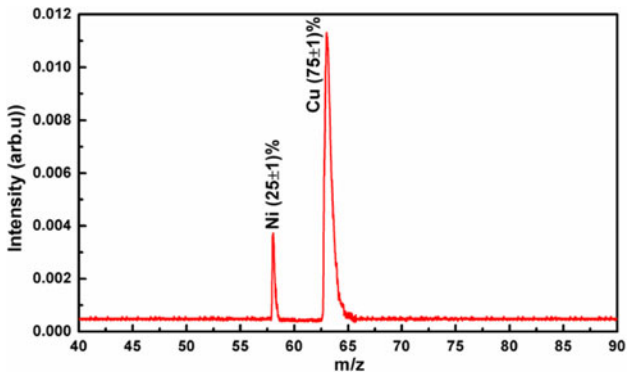

Fig. 6. Time of flight mass spectrum of the Cu–Ni alloy.

3.8. Quantitative Analysis by the Laser-Ablation TOF-MS, EDX and XRF Spectroscopy

Composition of the Cu–Ni alloy was also determined by the laser ablation-TOF-MS, EDX, and by the XRF technique. The spectrum acquired with a homemade one meter linear TOF-MS is shown in Figure 6. From the observed ion signal, the elemental composition has been determined as: Cu (74 ± 1%) and Ni (26 ± 1%). Incidentally, these values are in excellent agreement with the certified compositions.

The EDX spectrum of the Cu–Ni ally is reproduced in Figure 7. The presence of the constituent major elements in the sample is evident, showing Cu (75%) and Ni (24.5%). The analysis also yields the presence of a very small amount of Mn (0.4%) and Si (0.1%) in the EDX spectrum, which might be impurities on the surface of the sample.

The elemental analysis has also been performed by the XRF spectroscopic technique. The analysis yields the major elements present in the sample with composition of Cu (73%) and Ni (24.7%).

In Table 5, we enlist a comparison of the elemental compositions of the Cu–Ni alloy, which has been used to make the Pakistani five rupee coin, determined by the LIBS-based methods; OLCF-LIBS, SC-LIBS, CF-LIBS, and by the standard analytical techniques, LA-TOFMS, EDX, and XRF. The errors in the measured elemental compositions using

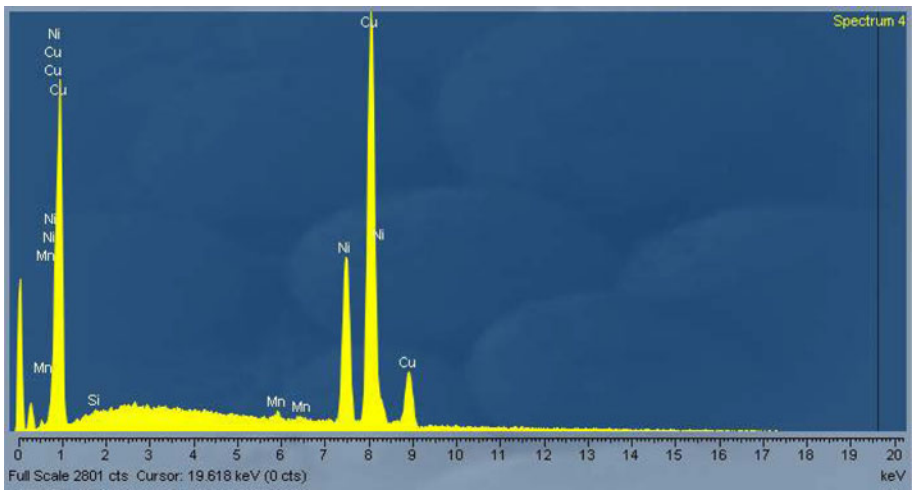

Fig. 7. Energy dispersive X-ray spectrum of the Cu–Ni alloy.

https://doi.org/10.1017/S0263034616000732 Published online by Cambridge University Press

Table 5. *Comparison of elemental compositions determined by different techniques.*

Composition (%)	OLCF-LIBS	SC-LIBS	CF-LIBS	EDX	XRF	LA-TOF
Cu	69	72	74	75	73	74
Ni	31	28	26	24.5	24.7	26

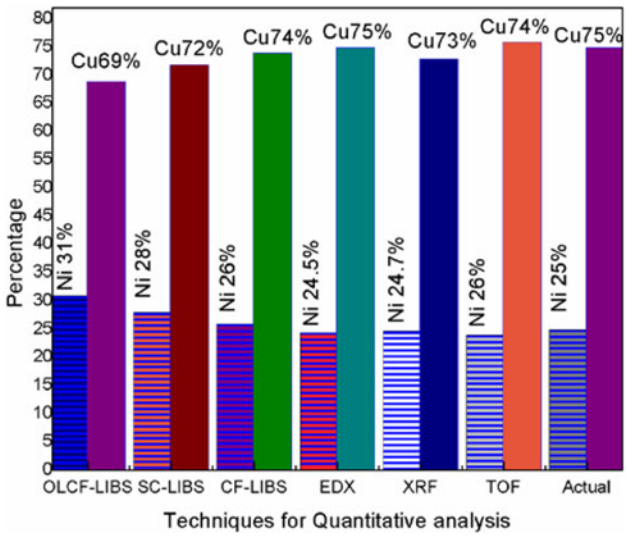

Fig. 8. Histogram across different techniques versus composition of Cu–Ni alloy.

the CF-LIBS method are comparable with that determined by the LA-TOFMS, EDX, and XRF analytical techniques.

To summarize all the data analyses, we present a comparison of different techniques in the form of a histogram in Figure 8.

4. CONCLUSION

In the present work, we have performed quantitative analysis of the Cu–Ni alloy (Pakistani Five Rupee Coin of year 2004) using three LIBS-based methods and three standard analytical techniques and compared the results with its certified composition. The one line CF method yields results containing about 6% error. The SC-LIBS method, which is based on the Boltzmann plot method contains about 3% error. The CF-LIBS method contains about 2% error. The elemental analysis using the LA-TOF, EDX, and XRF techniques yields much accurate results, with 1% error. The results of the CF-LIBS-based method are comparable with that of LA-TOF, EDX, and XRF revealing the importance of LIBS for a quick quantitative elemental analysis of any material.

ACKNOWLEDGMENTS

We are grateful to the Pakistan Academy of Sciences for the financial assistance to acquire the Laser system and the Higher Education Commission of Pakistan for the indigenous Ph.D. scholarship to Mr. Nasar Ahmed.

REFERENCES

Aguilera, J.A., Aragon, C., Cristoforetti, G. & Tognoni, E. (2009). Application of calibration-free laser-induced breakdown spectroscopy to radially resolved spectra from a copper-based alloy laser-induced plasma. *Spectrochim. Acta B* **64**, 685–689.

Ahmed, R. & Baig, M.A. (2009). A comparative study of single and double pulse laser induced breakdown spectroscopy. *J. Appl. Phys*. **106**, 033307.

Ahmed, R. & Baig, M.A. (2015). A comparative study of enhanced emission in double pulse laser induced breakdown spectroscopy. *Opt. Laser Technol*. **65**, 113–118.

Ahmed, R., Iqbal, J. & Baig, M.A. (2015). Effects of laser wavelengths and pulse energy ratio on the emission enhancement in dual pulse LIBS. *Laser Phys. Lett*. **12**, 066102–066107.

Andrea, E.D., Pagnotta, S., Grifoni, E., Legnaioli, S., Lorenzetti, G., Palleschi, V. & Lazzerini, B. (2015). A hybrid calibration free/artificial neural networks approach to the quantitative analysis of LIBS spectra. *Appl. Phys. B* **118**, 353–360.

Andrzej, W., Palleschi, V. & Israel, S. (2006). *Laser Induced Breakdown Spectroscopy (LIBS) Fundamentals and Applications*. New York: Cambridge University Press.

Babina, E.M., Ilinn, G.G., Konovalova, O.A., Salakhov, M.Kh. & Sarandaev, E.V. (2003). The complete calculation of stark broadening parameters for the neutral copper atoms spectral lines of 4s 2s-4p $2p^0$ and $4s^2$ 2d-4p $2p^0$ multiplets in the dipole approximation. *Publ. Astron*. **76**, 163–166.

Baig, M.A., Qamar, A., Fareed, M.A., Anwar-ul-Haq, M. & Ali, R. (2012). Spatial diagnostics of the laser induced lithium fluoride plasma. *Phys. Plasma* **19**, 063304.

Bassiotis, C., Diamantopoulou, A., Giannoudakos, A., Kalantzopoulou, F.R. & Kompitsas, M. (2001). Effects of experimental parameters in quantitative analysis of steel alloy by laser-induced breakdown spectroscopy. *Spectrochim. Acta B* **56**, 671–683.

Borgia, I., Burgio, L.M.F., Corsi, M., Fantoni, R., Palleschi, V., Salvetti, A., Squarcialupi, M.S. & Togoni, E. (2000). Self-calibrated quantitative elemental analysis by laser-induced plasma spectroscopy: Application to pigment analysis. *J. Cult. Herrit*. **1**, 281–286.

Bulajic, D., Cristoforetti, G., Corsi, M., Hidalgo, M., Legnaioli, S., Palleschi, V., Martins, J., McKay, J., Tozer, B., Wells, D., Wells, R., Harith, M.A., Salvetti, A., Tognoni, E., Green, S., Bates, D., Steiger, A., Fonseca, J. (2001). Diagnostics of high-temperature steel pipes in industrial environment by laser-induced breakdown spectroscopy technique. *Spectrochim. Acta B* **57**, 1181–1192.

https://doi.org/10.1017/S0263034616000732 Published online by Cambridge University Press

Burakov, V.S. & Raikov, S.N. (2007). Quantitative analysis of alloys and glasses by a calibration-free method using laser-induced breakdown spectroscopy. *Spectrochim. Acta B* **62**, 217–223.

Charfi, B. & Harith, M.A. (2002). Panoramic laser-induced breakdown spectrometry of water. *Spectrochim. Acta B* **54**, 1141–1153.

Ciucci, A., Corsi, M., Palleschi, V., Rastelli, S., Salvetti, A. & Tognoni, E. (1999). New procedure for quantitative elemental analysis by laser-induced plasma spectroscopy. *Appl. Spectrosc*. **53**, 960–964.

Cremers, D.A. & Radziemski, L.J. (2006). *Handbook of Laser-Induced Breakdown Spectroscopy, Handbook of Laser-Induced Breakdown Spectroscopy*. New York: Wiley.

Cristoforetti, G., Giacomo, A.D., Dell'Aglio, M., Legnaioli, S., Togoni, E., Palleschi, V. & Omenetto, N. (2010). Local thermodynamic equilibrium in laser induced breakdown spectroscopy: Beyond the Mcwhirter criterion. *Spectrochim. Acta B* **65**, 86–95.

De Giacomo, A., Dell'Aglio, M., De Pascale, O., Gaudiuso, R., Teghil, R., Santagata, A. & Parisi, G.P. (2007*a*). ns- and fs-LIBS of copper-based-alloys: A different approach. *Appl. Surf. Sci*. **253**, 7677–7681.

De Giacomo, A., Dell'Aglio, M., De Pascale, O., Longo, S. & Capitelli, M. (2007*b*). Laser induced breakdown spectroscopy on meteorites. *Spectrochim. Acta B* **62**, 1606–1611.

El Sherbini, A.M. & Saad Al Aamer, A.A. (2012). Measurement of plasma parameters in laser-induced breakdown spectroscopy using Si-lines. *World J. Nano Sci. Eng*. **2**, 206–212.

Fichet, P., Menut, D., Brennetot, R., Vors, E. & Rivoallan, A. (2003). Analysis by laser-induced breakdown spectroscopy of complex solids, liquids, and powders with an Echelle spectrometer. *Appl. Spectrosc*. **42**, 6029–6035.

Galbacs, G., Gornushkin, I.B., Smith, B.W. & Winefordner, J.D. (2001). Semi-quantitative analysis of binary alloys using laser-induced breakdown spectroscopy and a new calibration approach based on linear correlation. *Spectrochim. Acta B* **56**, 1159–1173.

Gomba, J.M., Angelo, C.D. & Bertuccelli, D. (2001). Spectroscopic characterization of laser induced breakdown in aluminum lithium alloy samples for quantitative determination of traces. *Spectrochim. Acta B* **56**, 695–705.

Gupta, G.P., Suri, B.M., Verma, A., Sunderaraman, M., Unnikrishnan, V.K., Alti, K., Kartha, V.B. & Santhosh, C. (2011). Quantitative elemental analysis of nickel alloys using calibration-based laser-induced breakdown spectroscopy. *J. Alloys Compd*. **509**, 3740–3745.

Hafeez, S., Sheikh, N.M. & Baig, M.A. (2008). Spectroscopic studies of Ca plasma generated by the fundamental, second, and third harmonics of a Nd:YAG laser. *Laser Part. Beams* **26**, 41–50.

Hahn, D.W. & Omenetto, N. (2012). Laser-induced breakdown spectroscopy (LIBS), Part II: Review of instrumental and methodological approaches to material analysis and applications to different fields. *Appl. Spectrosc*. **66**, 347–419.

Harilal, S.S., Shay, B.O. & Tillah, M.S. (2005). Spectroscopic characterization of laser-induced tin plasma. *J. Appl. Phys*. **98**, 0133061–0133067.

Hohreiter, V. & Hahn, D.W. (2005). Calibration effects for laser-induced breakdown spectroscopy of gaseous sample streams. *Anal. Chem*. **77**, 1118–1124.

Joseph, M.R., Xu, N. & Majidi, V. (1994). Time resolved emission characteristics and temperature profiles of laser induced plasmas in helium. *Spectrochim. Acta B* **49**, 89–103.

Konjevic, R. & Konjević, N. (1986). Stark broadening and shift of neutral copper spectral lines. *Fizica* **18**, 327.

Mohamed, W.T.Y. (2007). Calibration free laser-induced breakdown spectroscopy (LIBS) identification of seawater salinity. *Opt. Appl*. **37**, 1–2.

NIST. Atomic Spectra Database. http://physics.nist.gov

Noll, R., Begemann, C.F., Brunk, M., Connemann, S., Meinhardt, C., Scharun, M., Sturm, V., Makowe, J. & Gehlen, C. (2014). Laser-induced breakdown spectroscopy expands into industrial applications. *Spectrochim. Acta B* **93**, 41–51.

Noll, R., Bette, H., Brysch, A., Kraushaar, M., Monch, I., Peter, L. & Sturm, V. (2001). Laser-induced breakdown spectrometry applications for production control and quality assurance in the steel industry. *Spectrochim. Acta B* **56**, 637–649.

Shaikh, N.M., Kalhoro, M.S., Hussain, A., Baig, M.A. (2013). Spectroscopic study of a lead plasma produced by the 1064 nm, 532 nm and 355 nm of a Nd:YAG laser. *Spectrochim. Acta B* **88**, 198–202.

Singh, V.K. & Rai, A.K. (2001). Prospects for laser-induced breakdown spectroscopy for biomedical applications. *Lasers Med. Sci*. **26**, 673–687.

Tognoni, E., Cristoforetti, G., Legnaioli, S. & Palleschi, V. (2010). Calibration-free laser-induced breakdown spectroscopy: State of the art. *Spectrochim. Acta B* **65**, 1–14.

Tognoni, E., Cristoforetti, G., Legnaioli, S., Palleschi, V., Salvetti, A., Mueller, M., Panne, U. & Gornushkin, I. (2007). A numerical study of expected accuracy and precision in calibration-free laser-induced breakdown spectroscopy in the assumption of ideal analytical plasma. *Spectrochim. Acta B* **62**, 1287–1302.

Unnikrishnan, V.K., Alti, K., Kartha, V.B., Santhosh, C., Gupta, G.P. & Suri, B.M. (2010). Measurements of plasma temperature and electron density in laser-induced copper plasma by time-resolved spectroscopy of neutral atom and ion emissions. *Indian Acad. Sci*. **24**, 983–993.

Unnikrishnan, V.K., Mridul, K., Nayak, R., Alti, K., Kartha, V.B., Santhosh, C. & Gupta, G.P. (2012). Calibration-free laser-induced breakdown spectroscopy for quantitative elemental analysis of materials. *Pramana – J. Phys*. **79**, 299–310.

Winefordner, J.D., Gornushkin, I.B., Correll, T., Gibb, E., Smith, B.W. & Omenetto, N. (2004). Comparing several atomic spectrometric methods. *J. Anal. At. Spectrom*. **19**, 1061–1083.

https://doi.org/10.1017/S0263034616000732 Published online by Cambridge University Press